This paper has been published in SPIE APOC '07, Passive Components and Fiber-based Devices (Proc. 6781) and it is made available as an electronic preprint with permission of SPIE.

Advanced Topics on Fusion Splicing of Specialty Fibers and Devices

Invited Paper

B. S. Wang*, E. W. Mies
1400 Campus Drive, Morganville, NJ 07751, USA
bwang@vytran.com

ABSTRACT

The performance and integrity of optical fiber based devices and systems are often critically dependent on the optical coupling between interconnected fibers. In this paper, we discuss the optical characteristics of the interconnected joint when two dissimilar fibers are fusion-spliced together, and compare different approaches to estimate the optical coupling loss. We treat the total optical splice loss as a combination of the mode-field (MF) mismatch loss and the transition taper loss. We describe the spectral characteristics of mode-field mismatch loss and the taper loss between an erbium-doped fiber (EDF) and SMF28 fiber both experimentally and analytically. In addition, we outline some advanced techniques for fusion-splicing of large mode area (LMA) fibers and microstructured fibers. Finally, we compare two types of splicers using arc-discharge fusion and filament fusion technologies, and describe an automated splicing system with some examples.

Keywords: Fusion splicing, specialty fiber, large mode area fiber, microstructured fiber, EDF, wavelength-dependent loss, splice loss, splice transition, splice automation, optimization, simulation

1. INTRODUCTION

Fusion-splicing has been widely used to interconnect different optical fibers and devices. The splicing quality plays an important role on the performance and reliability of fiber devices and components in various fiber applications [(1), (2), (3)]. For erbium doped fiber amplifiers, a good optical coupling efficiency between fibers ensures high efficiency, flat gain spectrum, and low noise figure operation of the fiber amplifiers. In addition, the consistent and repeatable splicing leads to better manufacturing yield, thus lowers the production cost and improves throughput. Furthermore, the high mechanical strength at the splice joint is critical to ensure the excellent long-term fiber device reliability, which is essential for applications of undersea optical transmission and gyroscopes. Moreover, recent emerging specialty fibers, such as large mode area fibers and microstructured fibers pose a new challenge to the fusion-splicing technology because of their distinct fiber properties. New splicing techniques are required and more in-depth understanding of optical characteristics at the splice joints is required. Necessary splicing hardware needs to be developed to meet these challenges,

In this paper, we present some advanced topics and techniques on fusion splicing of specialty fibers. First, we describe fundamental optics at the fusion-spliced fiber joint and summarize different analytical approaches to estimate the light coupling at the splice. Second, we discuss, both experimentally and analytically, the spectral characteristics of the splice loss and the effect of the splice transition taper on the splice loss for dissimilar fibers. Third, we outline some advanced techniques for the optimal splicing of large mode area fibers and microstructured. Finally, we describe how fusion splicing technologies and hardware can evolve to meet the splicing challenges. We compare the arc-discharge fusion and filament fusion technologies and discuss the fiber splicing automation.

2. FUNDAMENTAL OPTICS AT SPLICE JOINT

When two dissimilar fibers are fusion spliced together, a longitudinally varying transition region at the splice joint is created. For a given fiber pair, the efficient light coupling between these two fibers depends on the proper optimization

of the splice joint. The waveguide transition at the splice joint leads to the optical field change when the light propagates through the splice. As a result, an optical transmission loss occurs at the splice joint.

A full quantitative description of the field propagation from one fiber to the other fiber through the splice transition region and the transmission loss estimation require solving the Maxwell's equations associated with corresponding boundary conditions based on the actual waveguide properties of two dissimilar fibers and the characteristics of splice transition. One approach is to use finite beam propagation method (BPM), which numerically solves the Maxwell's equation based on waveguide property in the vicinity of the splice.

It is convenient to decompose the total splice loss at the splice joint to two different parts, the mode-field (MF) mismatch loss and the transition taper loss. As shown schematically in Fig. 1, the taper loss occurs in the transition taper zone when the optical field of the propagating beam changes before it reaches to the other interconnected fiber. Generally, both interconnected fibers experience the transition loss during the splice depending on the fiber waveguide and doping properties. On the other hand, the mode-field mismatch loss occurs at the interface between two fibers because of the waveguide property difference at the vicinity of this interface. An example of the MF mismatch at the splice interface is also shown in Fig. 1. In addition to these two losses, losses due to light scattering and reflection occur at the splice joint. But these losses are generally significantly smaller,

The loss model outlined above offers a simplistic approach to estimate the light transmission at the splice joint. Both taper loss and mode-field mismatch loss can be estimated by using the beam propagation method (BPM) if the waveguide properties of interconnected fibers and the splice transition zone are known.

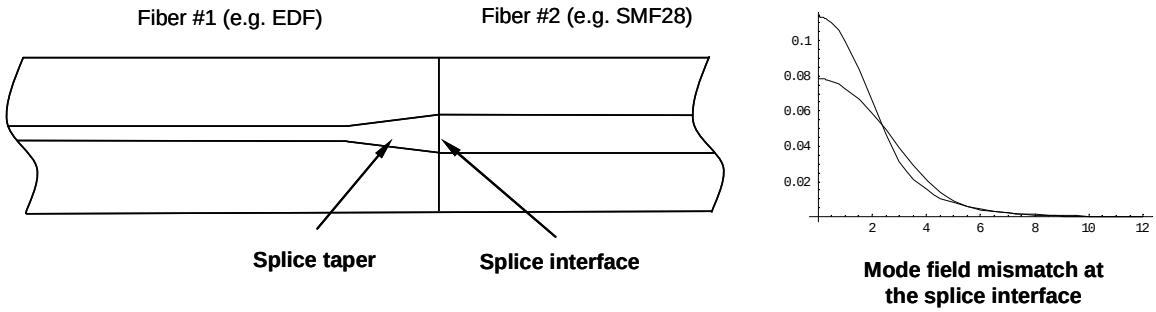

Fig. 1 Schematic of a splice joint formed by fusion-splicing of two dissimilar fibers

If the taper loss is neglected, the mode-field mismatch loss can be estimated based on the overlap integral of optical field amplitudes of the guided modes in the interconnected fibers using the following equation,

$$Loss\ (dB) = -10\log_{10}\left[\iint \varphi_1(r,\theta)\cdot\varphi_2(r,\theta)\,dr d\theta\right]^2 \quad , \tag{1}$$

where $\varphi_1(r,\theta)$ and $\varphi_2(r,\theta)$ are normalized field amplitudes of the guided modes for two fibers #1 and #2. If the fiber is single-mode and radially symmetric and has a step index core radius of "*a*" and refractive index of *NA*, the field amplitude of the fundamental mode then is [4]

$$\varphi(r) = \begin{cases} \dfrac{Y}{aV}\cdot\dfrac{J_0(r/a\cdot X)}{J_1(X)} & for \quad r < a \\ \dfrac{X}{aV}\cdot\dfrac{K_0(r/a\cdot Y)}{K_1(Y)} & for \quad r \geq a \end{cases} \quad , \tag{2}$$

where V is the fiber V parameter, which is defined as $2\pi aNA/\lambda$, J_0, J_1 and K_0, K_1 are Bessel and modified Bessel functions, respectively. Parameters X and Y are determined by the characteristics equation that satisfies the boundary conditions at fiber core/cladding interface.

To estimate the fundamental mode-field mismatch loss at the splice joint, the mode fields of two dissimilar fibers are firstly calculated using equation (2) and the loss is determined using equation (1). If the dopant diffusion or fiber geometry change occurs in the vicinity of the splice, the mode field calculation should be based on optical properties proximate to the splice interface. This overlap integral method does not account for any transition taper loss at the splice joint.

Sometimes, it is convenient to estimate the splice loss based on the mode field diameters of two connected fibers. If the mode field at the splice joint is further approximated by a Gaussian function, the loss at the splice joint can then be calculated by the following equation [5] considering the effect of fiber radial offset and fiber angular misalignment.

$$Loss\ (dB) = -10\log_{10}\left[\frac{2w_1w_2}{w_1^2+w_2^2}\right]^2 + 4.343\frac{2\delta^2}{w_1^2+w_2^2} + 4.343\left(\frac{2\pi n}{\lambda}\right)^2\frac{(w_1w_2)^2}{2(w_1^2+w_2^2)}\cdot\sin^2\theta \qquad (3)$$

where w_1 and w_2 are Gaussian spot radii of two fibers, δ is the radial offset of the fiber cores and θ is the angular misalignment of two fibers. Equation (3) includes the splice loss from the MF mismatch (1st term), the fiber core radial offset (2nd term), and the fiber angular misalignment (3rd term). The radial offset is associated with the fiber core eccentricity and the angular misalignment is attributed to the fiber cleave angle. In addition, the fiber alignment accuracy of the splicer could contribute to the radial offset and misalignment error.

Please note that the loss estimation from equation (3) is based on Gaussian approximation of the fiber mode field. This equation is often used to estimate the splice loss based on measured mode field radii of two fibers. This estimation works well when V numbers of two fibers at the splice joint are similar. When their V numbers are significantly different from each other, the calculation based on overall integral using equations (1) and (2) provides a better loss estimate. A comparison result using these two methods to estimate the fundamental MF mismatch loss from a 0.08-NA fiber to a 0.06-NA fiber with a core radius of 10μm is shown in Fig. 2. In the calculation, the core radius of the 0.08-NA fiber varies from 1μm to 18μm. The result shows that both methods agree well when the V numbers of two fibers are similar. Otherwise, the discrepancy could become significant.

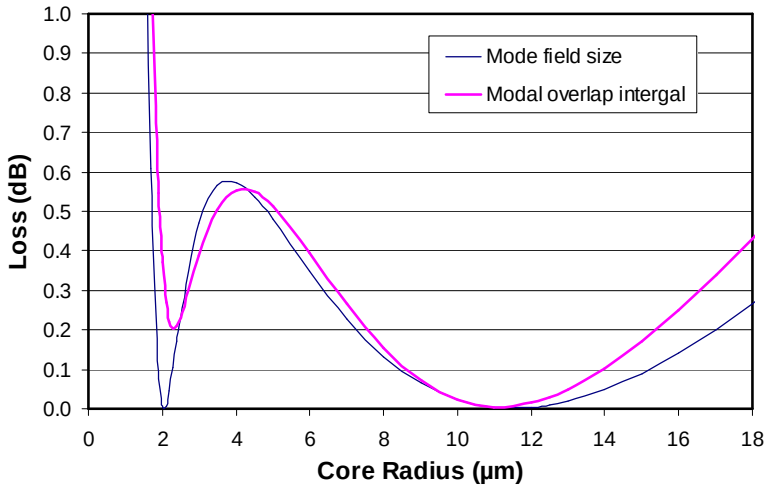

Fig. 2 Mode-field mismatch loss estimation comparison for different core radii of the fiber #1 with a 0.08-NA to the fiber #2 with a 0.06-NA and a core radius of 10μm

In summary, the beam propagation method provides a full description of the light propagation through the splice and its associated transmission loss. The overlap integral method estimates the mode-field mismatch loss of the guided mode propagation. With possible deviations, the loss calculation using the mode-field sizes of two interconnected fibers based on Gaussian approximation provides a simpler and more convenient way to estimate the coupling loss at the splice joint.

3. SPECTRAL CHARACTERISTICS OF THE SPLICE LOSS

For most applications, it is important to know the spectral characteristics of the splice loss. For erbium doped fiber amplifiers (EDFA), any spectral feature of the splice loss has a significant impact on the gain flatness, noise figure, and efficiency. The pump wavelength band (980 nm or 1480 nm) and the signal wavelength band (1550 nm) are significantly different. .In addition, the splice loss measurements are usually performed at around 1310 nm wavelength because of the negligible erbium absorption at this wavelength range. Therefore, full accurate description of the wavelength-dependent splice loss is essential for improving the fiber amplifier performance.

Because of the difficulty to measure the splice loss spectrally, the study in this area remains limited [6]. It is known that the transition taper length at the splice joint plays a significant role in the splice loss between two dissimilar fibers, and the efficient light propagation through the tapered region requires optimization of the optical property of the taper [7]. But effect of the splice taper on the spectral splice loss has long been neglected. In this section, we presented some results on spectral splice loss between an EDF and the SMF28 fiber using a well controlled splice loss measurement technique..

3.1 Spectral Splice Loss and Taper Loss Measurements

This study was to focus on the spectral splice loss between an erbium-doped fiber (EDF) and the SMF28 fiber for the wavelength ranging from 1.3 µm to 1.6 µm. In the splice loss measurement, we utilized the double-splice technique with the setup schematically shown in Fig. 3. For the spectral measurement, an ANDO white light source was used to launch a broadband light to SMF28 fibers. Before splicing in the EDF fiber, we measured the baseline spectrum using an ANDO optical spectral analyzer (OSA). Then both ends of a section of EDF were spliced to the SMF28 fibers. Another spectrum with the EDF spliced in was taken. As there is erbium absorption loss at around 1550 nm wavelength band, we precisely measured the EDF absorption spectrum beforehand. So, we can obtain the total wavelength-dependent splice loss between the EDF and the SMF28 simply by controlling the length of the EDF spliced with the SMF28 fibers.

It is also possible for us to determine the taper loss introduced by the EDF diffusion at the splice joint. (The taper loss due to the diffusion of SMF28 is small compared to that of the EDF. It is therefore neglected.) We first measured the baseline spectrum with a section of EDF fiber spliced in between the SMF28 fibers. Then we broke the middle of the EDF and two ends of the EDF were spliced together again. As two identical fibers were spliced together, the mode-field is always matched at the splice joint. So the splice generates negligible mode-field mismatch loss. The splice loss measured is therefore the taper loss induced by the EDF diffusion. In the measurements, the cleaved EDF length also needs to be accurately measured to remove the corresponding EDF loss due to the fiber length change before and after the splices.

Fig. 3 Setup for spectral splice loss measurement

3.2 Spectral Characteristics of the Splice Loss

The splice loss between dissimilar fibers is wavelength-dependent because of the dispersive nature of the silica fiber. Its spectral characteristics depends on the waveguide properties of the interconnected fibers, the dopant in the fiber cores, and the heat treatment at the splice joint when two fibers are fusion-spliced together. During splicing, the mode field diameter of the fiber expands due to the dopant diffusion, e.g. Al in EDF. This dopant diffusion helps to reduce the splice loss if the mode-field distribution of two fibers become better matched. In addition, because of the mode-field expansion, a transition region from a small mode-field to a large mode-field, or a taper, is created. This region induces additional optical transmission loss. Both MF mismatch loss and taper induced loss are wavelength-dependent.

To determine the spectral splice loss between the EDF and SMF28, we first estimated the wavelength-dependent splice loss due to the MF mismatch using equations (1) and (2) by taking the dopant diffusion into consideration. We assume that the dopant in the EDF diffuses with a constant V number, and the dopant diffusion in SMF28 is negligible. In the calculation, we assume the NA and the core diameter of the EDF are 0.23 and 1.5 µm, respectively, and the NA and the core diameter of the SMF28 fiber are 0.12 and 4.1 µm, respectively.

We calculated the wavelength-dependent loss due to MF mismatch between these two fibers in three cases: (1) when no diffusion occurs, (2) when optimal diffusion occurs, and (3) when the dopant diffusion is excessive. The result in Fig. 4 shows that MF mismatch loss changes from a negative spectral tilt to a positive tilt depending on the degree of diffusion or the MF expansion occurred at the splice joint. At the optimal MF matching condition, the wavelength-dependent loss is flat with a spectral variation of less than 0.01 dB.

Next, we calculated the MF mismatch loss vs. the degree of the diffusion, defined by the diffused mode-field radius, at both 1.3 µm and 1.55 µm wavelengths, as shown in Fig. 5. Based on this result, we can see that the loss does not reach minimum simultaneously at both 1.3 µm and 1.55 µm wavelengths. Therefore, optimal splice performance requires proper splice optimization.

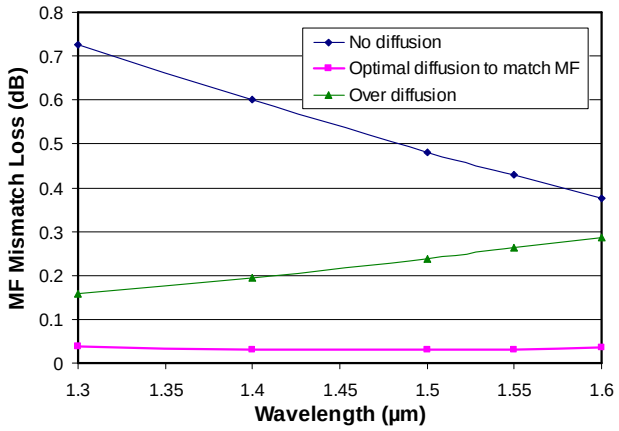

Fig. 4 Spectral MF mismatch loss with different diffusions

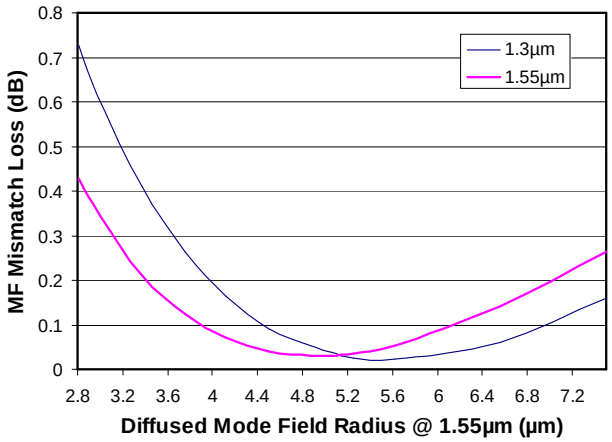

Fig. 5 MF mismatch loss at 1.3 µm and 1.55 µm

The wavelength-dependent taper loss can be determined either experimentally via the splice loss measurement or numerically using the beam propagation simulation method if the characteristics of the dopant diffusion and the splice taper are known. For the taper loss measurement, we used the measurement setup shown in Fig. 3 by splicing an EDF (OFS MP980 EDF) to itself. Spectral scans were taken before and after the splice using the optical spectral analyzer. As the mode-field between EDF to itself is always matched, the spectral loss due to the splice taper can then be determined from the loss difference between these two scans. The loss induced by the erbium absorption is properly subtracted out based on the cleaved EDF fiber length and measured erbium absorption spectrum.

We measured the spectral taper loss with different degrees of splice taper. We controlled the splice taper by introducing different heat treatment processes at the splice joint using a Vytran FFS2000 splicer, which allows fusion-scanning across the splice joint, called fire-polish. In the fire-polish process, the splicer head, a filament heater, moves back and

forward across the splice joint. The resulting heat treatment profile, the taper length and the degree of the taper can be programmed by setting up the fire-polish control parameters including the fire-polish length and the number of passes.

Using this approach, we measured the spectral taper loss in three different configurations: (1) 5-second fusion time with a 3-pass and 2mm-long fire-polish, (2) 5-second fusion time without fire-polish, and (3) 9- second fusion time without fire-polish. The measurement results given in Fig. 6 show that splicing using a fire-polish leads to a lower wavelength-dependent taper loss because the fire-polish method creates a relatively long smooth transition taper region. In addition, the excessive heating without the fire-polish generates high wavelength-dependent taper loss. A comparison between the measurement and the beam propagation simulation given in Fig. 7 shows a good agreement. As we can see from these results, the taper loss generates a positive spectral tilt. The loss and the magnitude of the tilt depend on the splice taper characteristics. A smooth taper transition and a long taper length as generated by using the fire-polish technique helps to reduce the taper induced loss and its wavelength dependency.

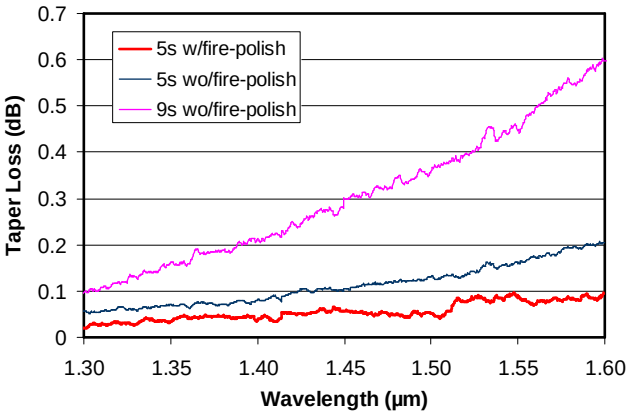

Fig. 6 Spectral splice tape loss at different fusion conditions by splicing the EDF to itself

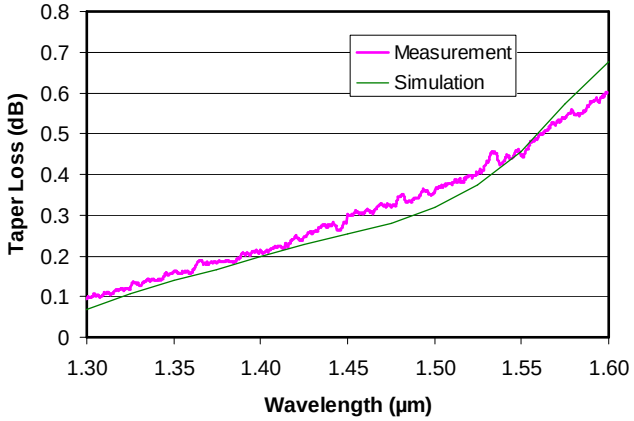

Fig. 7 Comparison between measurement and simulation

To further study the contribution of the splice taper loss to the overall splice loss, we measured the splice loss between the MP980 EDF and the SMF28 fiber at 1310nm wavelength with and without fire-polish enabled. The measurement was performed by splicing a section of EDF between SMF28 fibers using a setup similar to that in Fig. 3 but with a 1310nm signal source and a power meter instead of the white light source and the OSA. The splice loss measurements were made at different fusion times at two conditions with and without the fire-polish, respectively. The power of the splicer filament was set at 20.5W. With the fire-polish mode on, the splicer head additionally scans across the splice back and forward after the regular splicing is completed. In our setting, the splicer head scans across the splice three times, each with a total path length of 0.6 mm, 1.2 mm, and 1.8 mm, respectively. The comparison result of the splice loss at 1310nm with and without the fire-polish process shown in Fig. 8 indicates that the fire-polish mode indeed improves the splice loss. In addition, the splice loss is less dependent on the fusion time when fire-polish is used. The splice loss variation is 0.02 dB between 3-second and 6-second fusion time when the fire-polish is used, and it increases to 0.08 dB when fire-polish is not used. Therefore, a long smooth transition taper at the splice joint also helps to reduce the overall splice loss and improves the splice tolerance on fusion time.

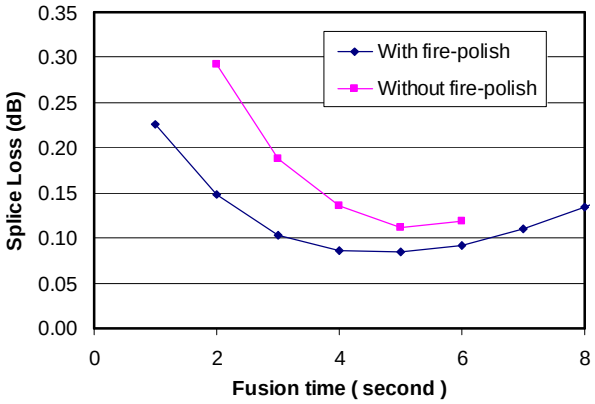

Fig. 8 Splice loss between EDF and SMF28 at 1310nm

To investigate the overall spectral splice loss due to both MF mismatch loss and the taper loss, we measured the wavelength-dependent loss by splicing a short section of EDF between the SMF28 fibers using the setup shown in Fig. 3. In the measurement, the EDF length spliced in was controlled precisely and the erbium induced loss is properly removed. The measured spectral splice loss in different conditions is shown in Fig. 9. In the case of the fire-polish (3-pass fire-polish) enabled, we measured the spectral loss of the splice with a fusion time of 4 seconds and a fusion power of 20.5 W. In this case, the average splice loss in the wavelength band from 1.3μm to 1.6μm is 0.08 dB, and the spectral loss variation is less than 0.02 dB. For comparison, we measured the spectral splice loss without the fire-polish with a fusion time of 3 seconds and 5 seconds, respectively. A positive tilt and a negative tilt are observed in these two cases. The result shows that a long smooth taper transition at the splice joint, as introduced by the fire-polish method, reduces the wavelength-dependent splice loss between the EDF and the SMF28 fiber.

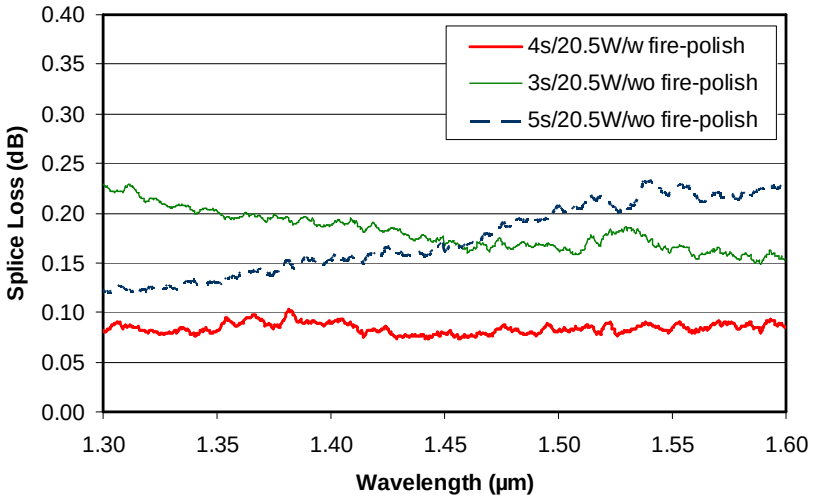

Fig. 9 Measured overall wavelength-dependent splice loss
(A long smooth transition splice taper reduces the wavelength dependent splice loss.)

From the above study on the wavelength-dependent splice results, we can reach following conclusions.

1) In order to reach a spectrally flat and low loss fusion splice between dissimilar fibers, e.g. EDF and SMF28, a proper optimization of both mode-field mismatch loss and the transition taper loss is necessary.

2) The MF mismatch loss generates a wavelength-dependent loss changing from a negative tilt to a positive tilt depending on the degree of the MF expansion. The lowest MF mismatch loss possible is generally depends on the waveguide properties of the two interconnected fibers, which can be estimated using the overlap integral method.

3) The taper loss depends on the heat treatment at the splice joint. The splice taper loss in the case of splicing between the EDF and the SMF28 introduces a positive spectral tilt. A long and smooth transition splice taper helps to mitigate this wavelength-dependent taper loss. A technique of scanning across the splice with a heat source after the splice is a useful technique to reduce splice taper loss and its wavelength dependency.

.

4. ADVANCED TECHNIQUES FOR OPTIMAL SPLICING OF SPECIALTY FIBERS

Various specialty fibers have been widely used for fiber amplifiers, lasers, dispersion compensation, and in telecom, fiber sensing and material processing applications. Recently, large mode area (LMA) fibers and microstructured become widely used because their lower nonlinearity and special optical property not available in conventional single-mode fibers. Fusion splicing of these fibers poses additional challenges. In this section, we outline some techniques for optimal-splicing of these two types of fibers.

4.1 Large Mode Area (LMA) Fibers

The LMA fiber usually has a low numerical aperture (NA) and in most cases supports a few modes. For example, a LMA fiber with a NA of 0.06 and a 10 µm core radius supports both LP_{01} mode and LP_{11} mode at 1.06 µm wavelength. Efficient coupling of light from a fiber with a small mode field to this type of LMA fiber is a major challenge for making LMA fiber devices. Different from EDF, the dopant, usually Ge, in these passive fibers does not have a good diffusivity. This limits the mode expansion capability during the fiber fusion splicing process. Several techniques, which include thermally expanded core (TEC) method, tapered fiber method, and the use of intermediate fiber, have been proposed to achieve better spliceability of LMA fibers to other fibers [7], [8].

TEC Method

Before the small MF fiber and the LMA fiber is spliced together, a heat treatment can be applied to the small MF fiber beforehand to expand its mode-field size by creating a low loss (or even lossless) transition taper. One example of the heat treatment is to scan the splicer head (a heat source) back and forward across the fiber with its coating removed. As most heat is applied to the mid of the fiber, the MF expands most at this point. The length of the transition taper depends on the scan length. The heat treatment profile can be programmed by setting up different process parameters. After the treatment, the fiber is cleaved precisely at the location where the mode-field size is the largest, ideally to match the mode-field of the LMA fiber. Finally, the cleaved fiber is spliced to the LMA fiber. Consequently, the optical coupling efficiency between these fibers can usually be improved because of the better mode-field match. However, the amount of beam expansion could be limited depending on the fiber design and the diffusivity of the fiber dopant. For the Ge doped single mode fiber, the mode-field expansion can generally be expanded by a factor 2-3.

The result of a mode field expansion example using the TEC method is shown in Fig. 10. The MFD of the single mode fiber at 1060 nm was increased from its original 6.4 µm to 9.3 µm and 12.8 µm, respectively, using two different treatments.

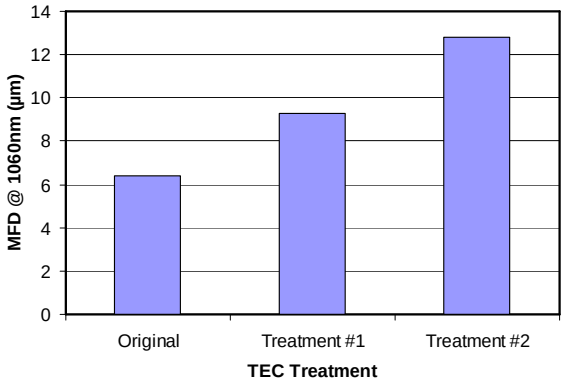

Fig. 10 MFD expansion example using TEC method

Fiber Tapering

Another method is to physically taper the small-mode field fiber. Different from the TEC method, the fiber tapering changes the core size of the fiber without altering the numerical aperture of the fiber. When tapering a fiber with a step-index core, the mode-field size decreases to reach a minima and then increases. An example of the calculated Petermann II mode-field radius versus the fiber core radius for a step-index fiber with a NA of 0.12 is shown in Fig. 11. The mode-field radius reaches a minimum at around 4 µm core radius. Reducing the core size further enlarges the mode-field, which possibly produces a lower loss coupling to a LMA fiber. An example of fiber taper image along with a mode-field change graph is shown in Fig. 12. The main drawbacks of this method are two-fold. First, as the fiber gets tapered, the cladding size becomes smaller. So its cladding size could become significantly different from the LMA fiber. This could cause fiber handling issue. Second, when the core gets smaller, the mode-field profile becomes significantly different from the LMA fiber even though the mode-field size matches perfectly. This could still introduce an excessive elevated optical coupling loss. In addition, the mode-field change also becomes drastic. This could cause a difficulty in tapering control.

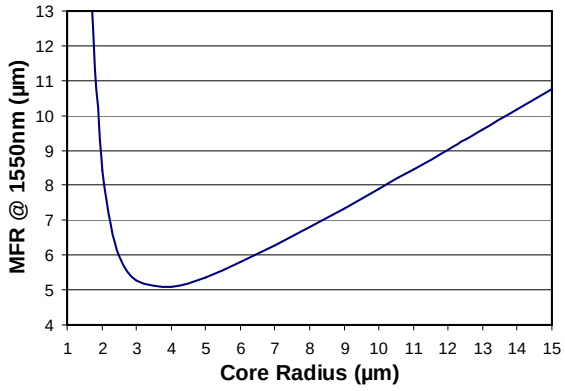

Fig. 11 MF radius vs. core radius for a fiber with 0.12 NA

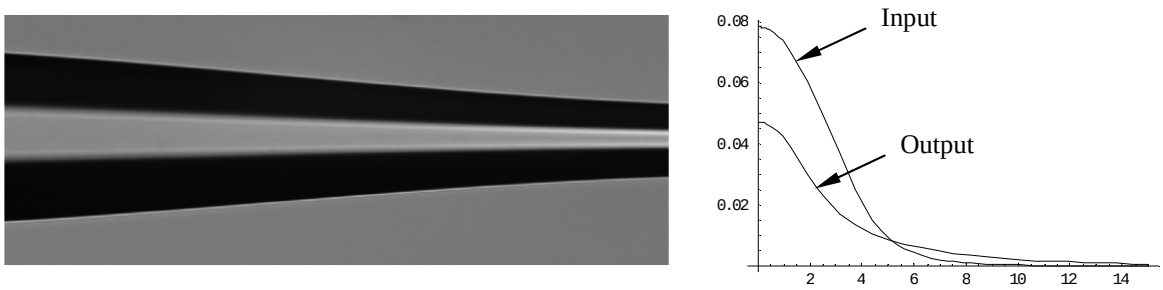

Fig. 12 A fiber taper image and the mode-field change due to tapering

4.2 Microstructured Fibers

Because of the inhomogeneous property of the microstructured fibers, both high quality cleaving and optimization of the splicing are required for a good optical coupling efficiency. In cleaving of a microstructured fiber, one major challenge is that cracks propagate at different speeds across different materials. As a result, it is possible that cracks do not grow evenly around the imbedded structure. In addition, any residual stress present in the imbedded elements can further perturb the crack propagation direction. One strategy to improve the cleave quality is to lower the crack propagation speed by reducing the fiber tension during cleaving and also reduce the size of the initial crack. However, a lower tension could result in a high cleave angle. So the optimization of the cleaving process is required. One approach to reach an optimized cleaving is following.

(1) Apply a tension to the fiber that is lower than that required for a crack to propagate (sub-critical tension)
(2) Scribe the fiber to initiate a crack
(3) Incrementally increase the tension and wait
(4) Repeat step (3) until the cleave is made

Two cleaved end face surface pictures of a microstructured fiber are shown in Fig. 13. The left picture shows an optimal cleaved surface using the process described above. The right picture shows the cleaved surface of the same fiber using a higher tension, which generates a non-ideal surface. Several surface fracture marks can be distinctly observed in this case.

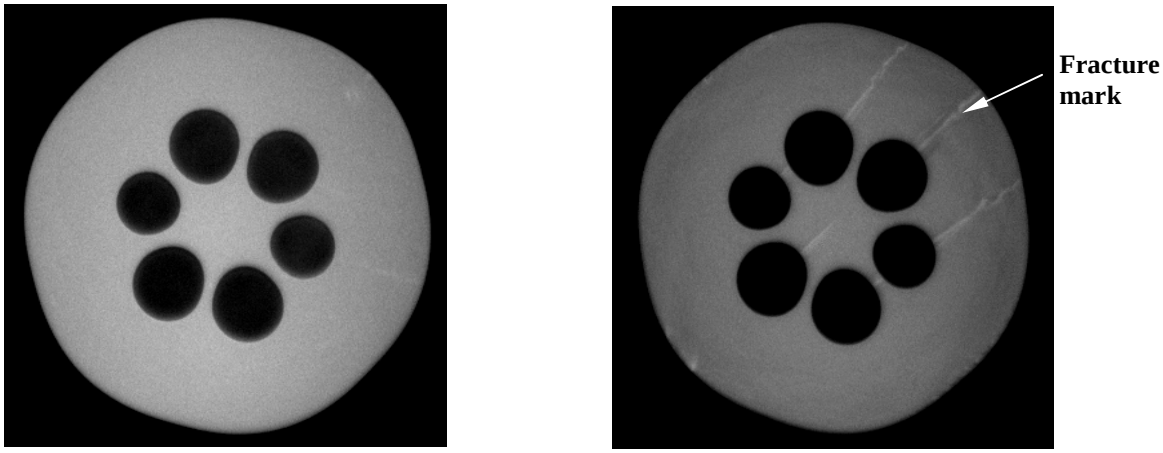

(1) optimal cleaving (2) high tension

Fig, 13 End face images of a microstructured fiber cleaved at different cleaving conditions

Fusion-splicing microstructured fibers to the conventional solid silica glass is pretty challenging as well, as their mode-fields are generally distinctly different. In addition, the heat treatment of the microstructured fiber can significantly alter its optical and mechanical properties. For example, air holes, the low index waveguide, in the air-hole fiber can collapse during the fusion splice process. This could lead to undesired optical waveguide property.

Several methods have been proposed to combat the challenges of splicing microstructured fibers [9], [10]. One good strategy is firstly to match the mode-field of the microstructured fiber using an intermediate solid fiber, e.g. a GRIN fiber lens or a fiber taper. Then the intermediate fiber is spliced to the microstructured fiber with a significantly reduced fusion temperature and time. This technique has shown to produce splices between the microstructured fiber and conventional fiber with both low loss and high mechanical splice strength [11].

5. SPLICING HARDWARD AND AUTOMATION

5.1 Arc-discharge Splicing vs. Filament Fusing Splicing

Two types of fusion splicing methods are available on commercially available equipment: arc-discharge splicing and filament fusion splicing. Additional splicing methods using high power laser [10] and flame fusion [12] have been developed for laboratory use.

The arc-discharge fusion splicers are mostly commonly used for splicing standard telecom silica fibers with a cladding diameter of 125 µm. This type of splicers uses the voltage applied across two seperated electrodes to generate current flow to heat up the area around the gap between these two electrodes. This type of splice is compact, portable, and it is easy to operate. The heating characteristics of the splicers depend on both the condition of electrodes and the ambient conditions, such as the temperature, humidity, etc. The electrodes need to be cleaned regularly to remove the silica particles or other contaminants accumulated on the electrodes. Otherwise, its splicing performance, e.g. splice loss and strength, could be compromised. In addition, the total heat produced by the splicer is not continous. The dynamic range of heat generated could be limited to achieve low heating or high heating splicing. So, the arc-discharge splicers are mostly suited for regular size fibers with the cladding diameter ranging from 125 µm to 250 µm. Because arc-dischage fusion splicer can be made very small and rugged, they are very well suited for field splicing applications.

Different from the arc-discharge splicer, the filament fusion splicer uses a resistently heated filament typically made of a refractory metal such as tungston as a heat source. The filament is usually a metal ribbon in a inverted Ω shape surrounding the inserted fibers, as shown in Fig. 14. A high purity noble gas purge is used to insure that the filament does not react with oxygen at high temperature. For the filament splicing, the heat generated can be tuned continuously over a wide temperature range. So fibers of different diameters ranging from tens of microns to milimeters in diameters can be fusion-spliced. In addition, the use of different types of filaments further expands its flexibility to accomadate various fusion splicing applications such as large mode area (LMA) fiber, microstructured fibers, PM fibers, fiber tapering, fiber couplers, and even fiber beam combining devices. High resolution image processing and precision multi-axis alignement stages are typically built in for accurate mechanical control and positioning of the fibers during splicing. A side-view image example of two aligned fibers is shown in Fig, 15. Though verstile, filament fusion splicers tend to be pricer than regular arc-discharge splicers, and because of their larger size and dependance on an inert gas supply, they are not ideal for field applications. They are best suited for production and specialty or high-end applications, such as LMA fiber splicing, high mechanical strength splicing, etc.

The latest fialment fusion splicers further increase and heat capacity and include fiber tapering as a standard process. This enables additional glass processing and device fabrication capabilities, such as fiber couplers, beam combiners, NA converters, mode-adaptors, and fiber lensing.

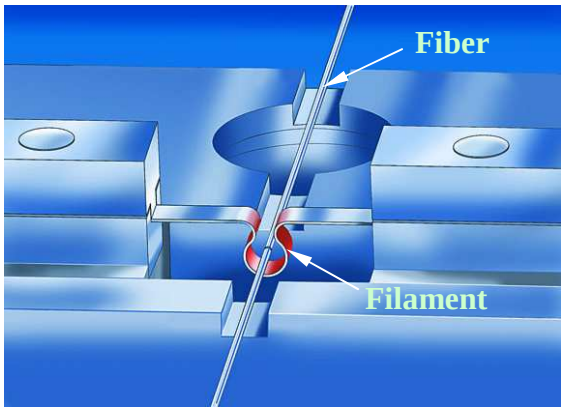

Fig. 14 Schematic of filament fusion splicing

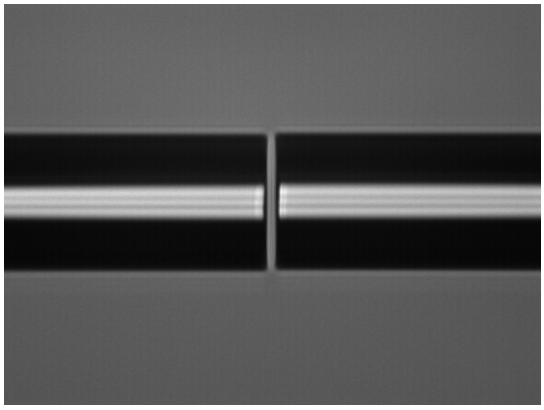

Fig. 15 Side-view image of two aligned fibers

5.2 Splicing Automation

Fiber fusion-splicing is a very labor-intensity repetitive process. The quality of the splicing depends not only on the splicer performance but also on the skill and experience of the operators. So the variation of splicing quality and performance is inevitable. Full splicing automation including fiber stripping, cleaving, splicing, testing, and even packaging can significantly improve the splicing quality, consistency, and yield, as operators do not need to touch the fibers any more during these processes.

Significant efforts have been made to automate the fusion splicing process. An example of the fiber automated system, FAS from Vytran, is shown in Fig, 16. The system only requires the operator to set up a fiber pallet with fibers to be spliced and then load the pallet to the machine. The rest including coating stripping, cleaving, splicing, splicing loss estimation or measurement, and recoating can be performed automatically without any operator involvement. The overall process per splice takes about 2 minutes on average. The system handles all common telecom fibers with a 125 µm cladding diameter, including EDF, DCF, PM fibers, and other undoped SM pigtail fibers. The system also has proof testing capability to test the mechanical strength of the splice. In addition, the system can fabricate fixed fiber attenuator and produce low reflection terminations such as ball lens terminations.

Fig. 16 An automated splicing system example

To evaluate the performance of the system, we statistically analyzed some automatically generated data, including the cleave angle, splice mechanical strength, and the splice loss. The cleave angle histogram distribution of over 7000 cleaves is shown in Fig. 17. Among these cleaves, the cleave angle is < 0.2 degrees for 75% of the cleaves and < 0.5 degrees for 97% of the cleaves, respectively. The small cleave angle insures the low splice loss, splice consistency, and high mechanical strength of the splices.

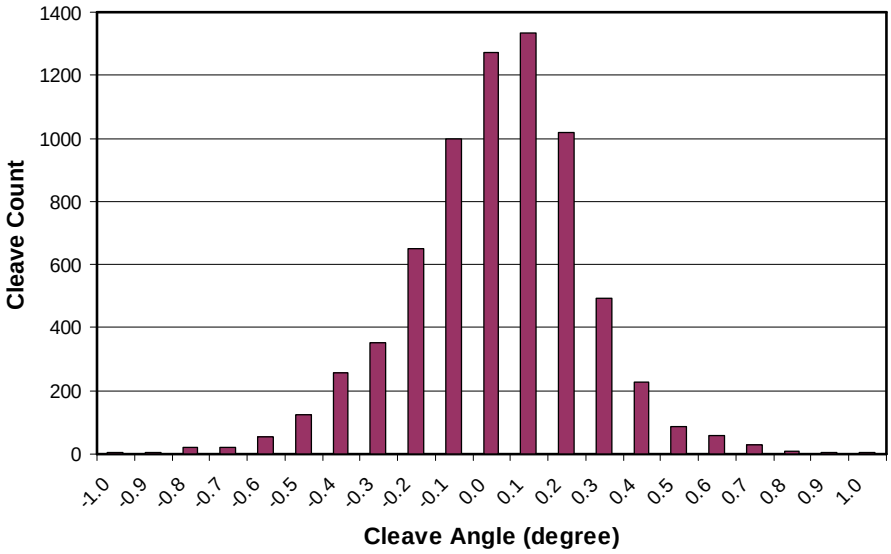

Fig. 17 Cleave angle histogram of over 7000 cleaves by the FAS system

The splice mechanical strength was evaluated for splices of SMF28-to-SMF28 and SMF28-to-EDF fiber pairs using the built-in proof test function. The splice strength histogram distributions of 100 splices of these two pairs are shown in Fig. 18. The average mechanical strength of these SMF28-to-SMF28 splices is 395 KPsi (2.72GPa) with a standard deviation of 110 KPsi (0.78GPa). For the EDF-to-SMF28 fiber pair, the average mechanical strength is 377 KPsi (2.6GPa) with a standard deviation of 96 KPsi (0.67GPa). The mechanical strength of these splices is higher than the typical proof test level of these fibers, which is usually between 100 KPsi (0.69 GPa) and 200 KPsi (1.38 GPa). The high mechanical strength of splices is critical for long-term reliability of fiber devices, such as EDFA and ASE source in telecom and gyroscope applications.

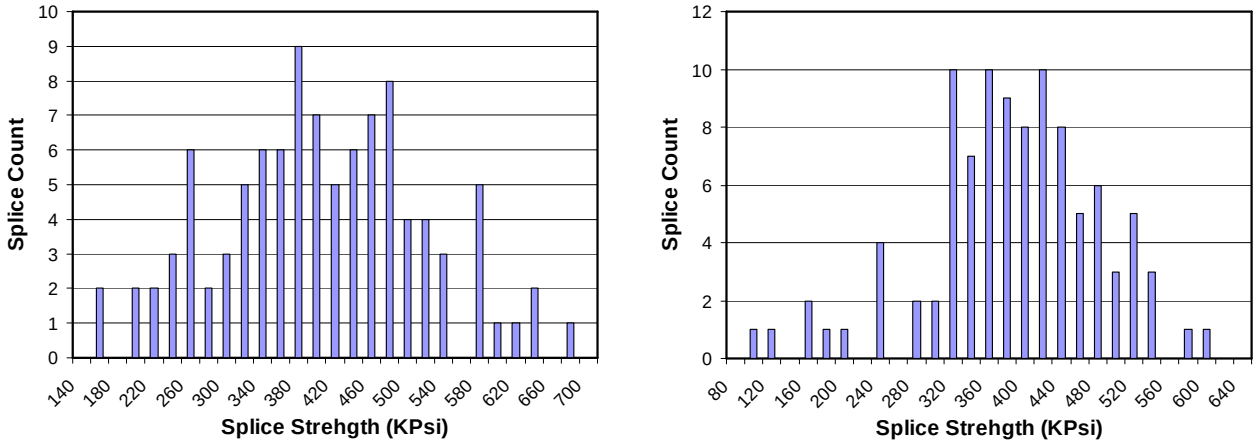

SMF28-to-SMF28
(average strength 395 KPsi, or 2.72GPa)

EDF-to-SMF28
(average strength 377 KPsi, or 2.60GPa)

Fig. 18 Mechanical strength distributions of splices between SMF28 to SMF28 and EDF to SMF28

In addition, we measured and analyzed the splice loss for SMF28-to-SMF28 and EDF-to-SMF28 splices at 1550nm. The average loss for the SMF28-to-SMF28 fiber pair is 0.016 dB with a standard deviation of 0.006 dB for 50 splices. The

measured splice loss result of 50 splices for a EDF-to-SMF28 pair is shown in Fig. 19. The average splice loss at 1550nm is 0.21 dB with a standard deviation of 0.01 dB. The consistency of the splice loss between EDF and SMF28 and other fiber pairs is important to insure the high EDFA performance and manufacturing yield.

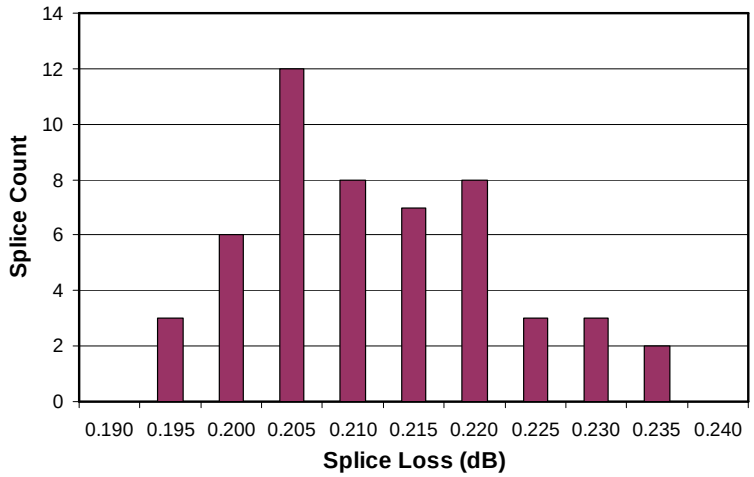

Fig. 19 Measured splice loss at 1550nm between a EDF and the SMF28 fiber (average splice loss 0.21 dB, and 1σ 0.01 dB)

6. CONCLUSIONS

We described fundamental optics at the splice joint of dissimilar fibers with a focus on the evaluation of splice loss using different methods. The BPM method provides full description of both MF mismatch loss and taper loss at the splice joint. The overlap integral method only accounts for the MF mismatch loss. This approach provides a more rigorous prediction than the method which uses the Gaussian mode field estimate.

The study on the wavelength-dependent splice loss between EDF and SMF28 showed that both MF mismatch loss and transition taper loss at the splice joint are wavelength-dependent. It is essential to have a proper heat treatment to create an optimal splice transition taper to reduce the taper induced loss, thus lowering the overall wavelength-dependent splice loss. A low and flat splice loss across a wavelength band between 1.3 µm and 1.6µm has been demonstrated.

In addition, we outlined some advanced splice optimization techniques for fusion-splicing specialty fibers such as LMA fibers and microstructured fibers. TEC and fiber tapering are two useful methods to improve the coupling efficiency between different specialty fibers. A strategy to cleave the microstructured fiber by properly controlling the crack initiation and the tension applied was introduced.

Finally, we discussed splicing equipments and splicing automation. The filament based fusion splicing technology offers a wide heat treatment range. It is therefore suitable for various high-end applications, such as LMA and microstructured fibers as well as applications that require high mechanical strength at the splice joint. Splicing automation provides the ultimate solution for the manufacturing yield and consistency improvement of fiber devices.

7. ACKNOWLEGEMENT

The authors thank Bob Swain and Mike Harju of Vytran for providing measurement data and fiber process images. The authors also acknowledge Jim Moore of OFS Fitel at Somerset, New Jersey, for providing the MP980 EDF fiber sample.

8. REFERENCES

1. A. D. Yablon, *Optical Fiber Fusion Splicing*, Springer, (2005)
2. M. Nakano, et. al., "Improvements in splicing dissimilar fibers for dispersion-managed ultra long haul network," Proc. 51st IWCS, (2002)
3. G. Kweon, et. al., "Splicing losses between dissimilar optical waveguides," Journal of Lightwave Technology, **17**, 690, (1999)
4. D. Gloge, "Weakly guiding fibers," Appl. Opt., **10**, 2252, (1971)
5. E. G. Neumann, *Single-Mode Fibers: Fundamentals*, Springer-Verlag, Berlin, (1988)
6. H. Seo, et. al., "Gain and noise figure improvement of erbium-doped fiber amplifiers by optimizing spectral splicing conditions," OFC Technical Digest, WM48, (1998)
7. C. D. Hussey, K. P. Oakley, "Low-loss splices between different fibres," Proc. SPIE **4876**, Optics and Photonics Technologies and Applications, Thomas J. Glynn, Editor, (2003)
8. A. D. Yablon, "Optimal design of intermediate fibers," OFC Technical Digest, OWI3, (2007)
9. B. Bourliaguet, et. al., "Microstructured fiber splicing," Opt. Express, **11**, 3412, (2003)
10. J. H. Chong, et. al., "Development of a system for laser splicing photonic crystal fiber," Opt. Express, **11**, 1365, (2003)
11. A. D. Yablon, R. T. Bise, "Low-loss high-strength microstructured fiber fusion splices using GRIN lenses," Photonic Tech. Lett., **17**, 118, (2005)
12. J. Krause, "Method for glass fiber splicing by flame fusion," US patent, US4713105, (1987)